Science Press

Enhanced Sensing Properties of Acetone with Hollow Porous NiO/SnO$_2$ Nanocomposites Decorated by Carbon Nanotubes

Zhou Honglei,   Chen Xiaohong,   Fan Jun,   Liu Ping

School of Materials Science and Engineering, University of Shanghai for Science and Technology, Shanghai 200093, China

Abstract: The hollow porous NiO/SnO$_2$ composite nanofibers were prepared by electrospinning method, then the carbon nanotubes (CNTs) were decorated on the surface of the composite fibers, marked as CNTs/NiO/SnO$_2$. On this basis, a gas sensor device was prepared. The thermal decomposition temperature and heat treatment process of the composites were determined by TGA. The morphology, structure, size and surface composition of the composites were characterized by SEM, XRD, TEM and XPS. The test results of the gas sensors based on the composites show that the gas sensor prepared by CNTs NiO/SnO$_2$ composite nanomaterial reduces the optimum working temperature in detecting acetone gas, which is 160 °C, and the composite nanomaterial also improves the detection sensitivity. The gas sensors based on CNTs/NiO/SnO$_2$ have a good response to 50 μL/L acetone, reaching 25.25, and quick response to the detection of acetone (~8.2 s) with a recovery time of only ~10.5 s, and also show good stability in the 30 d long-term stability test. The potential value of NiO/SnO$_2$ composites with decorative CNTs in the detection of acetone was proved. At the same time, the mechanism of the improvement of detection performance of CNTs and hollow porous structure NiO/SnO$_2$ was discussed.

Key words: NiO/SnO$_2$; semiconductors; carbon nanotubes; gas sensors

Acetone is a kind of organic compound with slight toxicity and it is widely used in industrial production. Exposure to acetone for a long time will cause harm to human body. Acetone can be absorbed through the respiratory tract, digestive tract and skin. Exposure to high concentrations of acetone can cause damage to the liver, kidneys and pancreas of the human body. Therefore, in order to ensure the safety of people's work, it is urgent to develop a new method for efficiently detecting acetone gas. Common methods for detecting acetone are based on catalytic luminescence[1-3], fiber optic sensors and infrared analyzers[4,5]. In the past few decades, gas sensors based on SnO$_2$, ZnO and α-Fe$_2$O$_3$ with high sensitivity, real-time dynamic detection and low power consumption, have been considered as a promising sensor material[6-10]. Although these oxides have made significant progress, meeting the growing demand such as low operating temperatures, rapid response and recovery speed, there are still challenges[11]. In a word, a lot of improvement studies have been carried out, in-

cluding the novel material structure designing, loading with precious metals[12,13] and doping transition metals[14,15]. Zhang et al[16] reported a simple method for synthesizing porous NiFe$_2$O$_4$ microspheres by combining a one-step solvothermal route with a heating annealing procedure. The experimental results show that a gas sensor based on porous NiFe$_2$O$_4$ microspheres shows high response (27.4) to 100 μL/L acetone, low response detection limit (200 μL/L), and excellent repeatability at an optimum operating temperature of 250 °C. Liu et al[17] developed an acetone sensor by decorating Pt NPs on the surface of Al-doped ZnO NPs, to realize improved sensing properties such as high sensing response, rapid response time, and good selectivity.

Metal oxide semiconductor (MOS) sensing materials have attracted great attention due to their structural stability, high sensitivity and low cost[18-20]. Among all MOS, SnO$_2$ is a very popular n-type semiconductor sensing material with wide band gap (E_g=3.6 eV), which is mainly used to measure oxida-

tion and reduction gases[21], but pure SnO_2 sensitive material cannot meet the requirement for high-sensitivity detection of toxic gases, and its preparation is generally carried out at higher temperature. In this work, NiO as an important p-type semiconductor was selected as a second metal oxide coupled with SnO_2. In the previous research, we have reported that CuO-SnO_2 nanofibers doped with 3wt% CNTs show the best responses to H_2S with short response and recovery time, while reducing the optimal operating temperature[22]. Zhang et al [23] presented a solvothermal strategy to synthesize $W_{18}O_{49}$ UFNWs with a diameter of only 0.8 nm. The obtained UFNWs have only one well-defined [010] exposed plane, more vacancy oxygen and adsorbed oxygen, and large specific surface area about 194.72 m^2/g. The UFNWs exhibit ultrahigh acetone selectivity and sensitivity. In this study, hollow porous NiO/SnO_2 nanoheterojunctions were formed by electrospinning, and 3wt% CNTs were added to decorate NiO/SnO_2 nanofibers. The sensing mechanism for acetone was also discussed in detail.

1 Experiment

1.1 Preparation of NiO/SnO_2 composite nanofibers

In this work, polyvinylpyrrolidone (PVP) with the molecular mass of 1 300 000, DMF (N, N-dimethylformamide), Ni-$Cl_2 \cdot 2H_2O$, $SnCl_2 \cdot 2H_2O$, acetone (CH_3COCH_3), ethanol (C_2H_5OH), cetyltrimethylammonium bromide (CTAB), CNTs, H_2SO_4 and HNO_3 were purchased from Sinopharm Chemical Reagent Co., Ltd. All the chemicals used were analytically pure. First, 1 g PVP was added into some amount of DMF. Then the solution was under intense magnetic stirring for 2 h at 60 °C until the solution was clear. Next, a certain quality of $NiCl_2 \cdot 2H_2O$ and $SnCl_2 \cdot 2H_2O$ (SnO_2, NiO molar ratio 1:1) were added into the solution and continued to stir at 60 °C until the mixed solution was uniform. Meanwhile, the pure polymer solution without adding $NiCl_2 \cdot 2H_2O$ and $SnCl_2 \cdot 2H_2O$ was obtained by the same way. Finally, the homogeneous solution as shell layer and pure polymer solution as inner layer were transferred into two syringes with a stainless steel coaxial electrospinning needle (core inner diameter 0.41 mm, shell inner diameter 1.01 mm). The distance between the tip of the syringe needle and the collector of the Al plate covered by aluminum foil was fixed in the range of 15~20 cm and the feeding rates of internal and external layer were adjusted at a constant rate of 0.0005 and 0.0009 mm/s, respectively. The applied voltage between the tip and the Al plate was maintained at 18~22 kV. After electrospinning, the nanofibers were dried at 80 °C for 12 h, then calcined at 260 °C in air for 30 min with a heating rate of 2 °C/min, and then continued to be calcined at 600 °C for 2 h with the same heating rate to decompose organic matter and salt completely in order to get NiO/SnO_2 nanofibers, and this progress was directed by the result of TGA test. Schematic diagrams of the electrospinning device and coaxial electrospinning needle are shown in Fig.1.

1.2 Synthesis of CNTs/ NiO/SnO_2 composite nanofibers

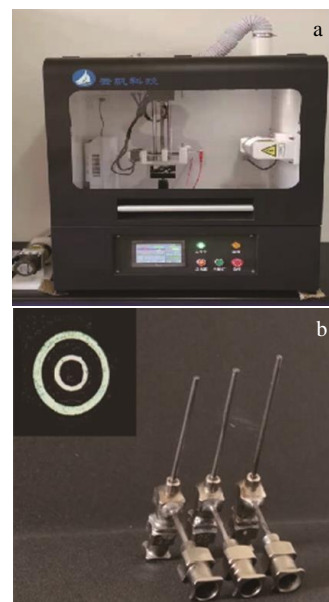The acidified CNTs were prepared by heating reflux

Fig.1 Schematic setup of electrospinning：（a）electrospinning device and（b）coaxial electrospinning needle

method in acid solution. In a typical process, weigh 0.5 g CNTs and add 20 mL H_2SO_4 and 60 mL HNO_3, and stir in water bath environment at 90 °C for 3 h. The cooling sample was taken out from the water bath, and then centrifuged after the temperature drops to room temperature. The acidified CNTs were diluted with water to about 200 mL, and poured into a centrifuge tube to be centrifuged to neutral; the centrifuged carbon tube was ultrasonically dispersed in two portions. 0.2 g CTAB was added into each portion for dispersion in an ultrasonic disperser, and the disperser was set to a power of 50% for 60 min. Finally, the calcined nanofibers were added by 3wt% acidified CNTs, and the sensor materials were obtained.

1.3 Material Characterization

The morphology of the nanocomposites was obtained by SEM (FEI, Quanta FEG 450, USA). The crystal structure of NiO-SnO_2 nanocomposites was analyzed by X-ray diffraction (XRD, Breker, D8 Advance, Germany) with Cu-Kα ($\lambda = 0.154\,18$ nm) radiation, with a scanning speed of 5°/min and 2θ of 20°~90°. The transmission electron microscopy (TEM) images and high-resolution transmission electron microscopy (HRTEM) images were gained by a Tecnai G220S-Twin transmission electron microscope. The thermogravimetric (TG) analysis was carried out in dynamic air atmosphere (75 mL·min^{-1}) with a heating rate of 2 °C·min^{-1} using Pyris 1 TGA thermal analyzer. The specific surface area of the powders was characterized by Brunauer-Emmett-Teller (BET) method. Surface elemental analysis was performed by X-ray photoelectron spectroscopy (XPS, Thermo Scientific, and ESCALAB 250).

1.4 Fabrication of gas sensing device

The composite material treated with 600 °C heat annealing preservation was dissolved in absolute ethanol for grinding treatment, and coated on ceramic tubes, and the resistance

wires were introduced into the ceramic tubes to perform the heat treatment, and the prepared sensor member was aged on the gas sensor aging table for 12 h. The samples were mixed with ethanol to form a paste. Sensors were made by uniformly coating the paste on a ceramic tube. And an electrode was installed at both ends of the ceramic tube, and each electrode was connected by two Pt wires, and a Ni-Cr resistance wire was inserted into the ceramic tube in order to heat the sensor. For semiconductor metal oxide sensors, the resistance varies with the operating temperature of the sensor element. When the air and gas to be tested contact the surface of the sensing element, the resistance will also change. The corresponding steady-state resistance in the air environment is defined as R_{air}, and the corresponding steady-state resistance in the gas environment to be tested is defined as R_g, which is recorded separately. The sensitivity of the gas sensor device to be measured is determined to be R_a/R_g. After the test gas is poured into the test room, the time of sensor resistance reaching the steady state is defined as the response time; the test gas is turned off and flushed with the air, and the time required for the resistance returning to 90% of the resistance before the gas is tested is taken as the recovery time. Schematics of the gas sensor and gas sensing test circuit are shown in Fig.2.

2 Results and Discussion

2.1 Morphology, structure and thermal stability

The morphology of the original composite nanofibers is shown in Fig.3. As can be seen from Fig.3a, the nanofibers have a smooth and nearly uniform surface. The inset of Fig.3a shows a corresponding high magnification image, clearly showing the nanofibers with a diameter about 400 nm. The
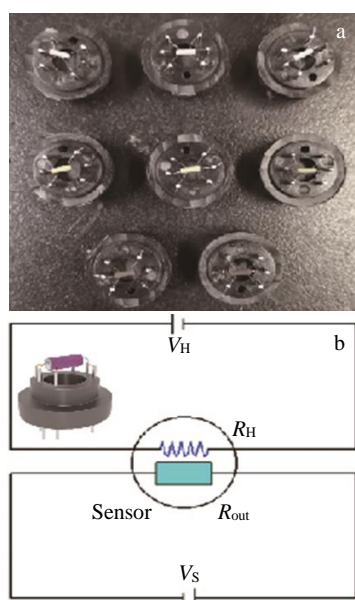

Fig.2   Schematic of gas sensor device（a）; gas sensing test circuit and 3D model in the insert（b）（R_H: heat resistance; R_{out}: signal resistance; V_H: heating voltage; V_S: circuit voltage）
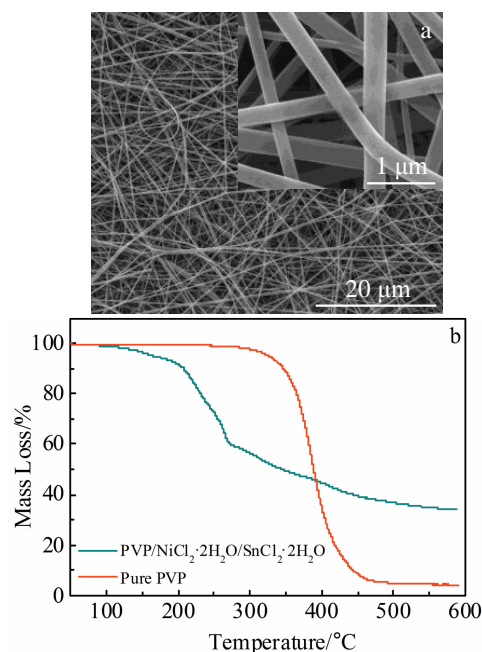

Fig.3   SEM morphology of as-spun NiO/SnO$_2$ prepared by electrospinning（a）and TGA curves of NiO/SnO$_2$ precursor fabricated by electrospinning（b）

TGA characterization of the electrospinning precursor is shown in Fig.3b. The first stage is 50~200 °C, and the decomposition is about 10%. The solvent is mainly volatilized on the composite fiber. The second stage is 200~260 °C, in which NiCl$_2$, SnCl$_2$ and polymer PVP branch decomposition occurs. The third stage 260~500 °C, in which polymer PVP is completely decomposed, the sample mass is almost unchanged after 500 °C, and the remaining material is pure inorganic, metal oxide, corresponding to an exothermic peak at about 330 °C. As the temperature increases to 500 °C, the system mass remains unchanged, indicating that an annealing temperature of 600 °C is reasonable to be chosen. The chosen temperature not only ensures that no organic impurities are present in the product, but also ensures sufficient crystallinity[24]. If the annealing temperature is too high, the specific surface is significantly reduced, resulting in a decrease in gas response [25].

Fig.4a shows the morphology of the fibers after annealing at 600 °C for 2 h in air atmosphere (heating rate is 2 °C/min, the temperature is raised to 260 °C for 30 min). It is apparent that the fiber diameter is reduced, and according to statistical data, the diameter is about 300 nm owning to the decomposition of PVP and the conversion of the precursor to the NiO/SnO$_2$ composite. According to the SEM morphology, it can be seen that the precursor fiber is decomposed into coarse hollow nanorods composed of nanoparticles. The hollow structure increases the surface area per unit volume, and the rough surface provides a large number of attachment sites for the gas. The XRD pattern with a 2θ range of 20°~90° for the calcined sample is shown in Fig.4b. It can be seen that all the diffraction peaks are NiO or SnO$_2$ crystal planes. According to
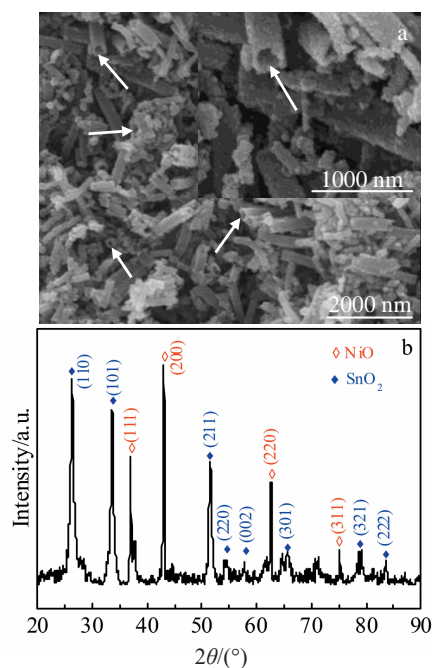
Fig.4　SEM morphology（a）and XRD pattern（b）of as-spun NiO/
SnO$_2$ fibers annealed at 600 ℃ for 2 h in air

the XRD results of the composite, it can be proved that the two phases of NiO and SnO$_2$ coexist in the product, which provide the possibility of forming a nanoheterostructure at the interface between NiO and SnO$_2$.

In order to further study the NiO/SnO$_2$ composites decorated with CNTs, the microstructure of the composite is shown in Fig. 5. As can be seen from Fig. 5a, the low magnification TEM image clearly shows the microscopic morphology of the individual nanofiber after calcination treatment, while near the fibers, there are CNTs (about 20 nm in diameter). And it can be seen in the inset of Fig. 5a that the nanofibers have a bright field of the edge dark field core, further demonstrating that the fibers have a hollow structure. The high resolution transmission electron microscope (HRTEM) image shown in Fig. 5b reveals the coexistence of NiO and SnO$_2$ crystals in the CNTs/NiO/SnO$_2$ composite fiber. According to the HRTEM image

results, the interplanar spacing of 0.335 and 0.265 nm corresponds to the [110] and [101] crystal faces of the tetragonal rutile structure of SnO$_2$ [19], respectively. In addition, the interplanar spacing is 0.241 nm and the spacing is consistent with the [111] plane of NiO with monoclinic crystals[26,27]. It is apparent from these results that each of the nanoparticles consists of a single phase of NiO or SnO$_2$ phase, rather than a solid solution phase of NiO/SnO$_2$. This indicates that the NiO/SnO$_2$ nano-heterojunction in CNTs/NiO/SnO$_2$ nanomaterial is successfully achieved.

Fig. 6 shows the experimental and fitted photoelectron spectroscopy of Cu 2p, O 1s and Sn 3d. In Fig.6a, all peaks on the curve are assigned to the C, O, Cu, and Sn elements, and no peaks of other elements are observed. Fig.6b shows the Ni 2p spectrum of the composite. The Ni 2p signal can be deconvoluted into four peaks at 855.8, 861.6, 873.8 and 879.7 eV. The binding energy at 855.8 and 861.6 eV can be attributed to the Ni 2p$_{3/2}$ peaks, and the 873.8 and 879.7 eV peaks are attributed to Ni 2p$_{1/2}$ [28]. The XPS spectra of pure SnO$_2$ and composite nanofibers for Sn 3d show two peaks in Fig.6c; 486.9 eV is assigned to the spin orbit of Sn 3d$_{5/2}$, and 495.3 eV corresponds to Sn 3d$_{3/2}$. In addition, Sn 3d$_{5/2}$ and Sn 3d$_{3/2}$ (the difference in binding energy 8.5 eV) are also in good agreement with the standard data of the tetravalent oxidation state in SnO$_2$, corresponding to Sn^{4+} in a tetragonal rutile structure[26]. The O 1s peak of the CNTs/NiO/SnO$_2$ composite is well fitted by Gaussian distribution in Fig.6d. The main O 1s peak can be attributed to oxygen in the NiO, SnO$_2$ lattice. The O ad peak should be attributed to O$^-$ ions and O^{2-} ions in the oxygen deficient region caused by oxygen vacancies[25]. Based on the above results, it can be concluded that the CNTs/NiO/SnO$_2$ nanocomposites are composed of Ni^{2+}, Sn^{4+} O, and C.

2.2 Gas-sensing properties

Fig. 7a shows the typical response of sensors based on CNTs/NiO/SnO$_2$ and NiO/SnO$_2$ composites to volatile acetone at different temperatures. The response is the function of the temperature, and the temperature at which the response reaches its maximum is called the optimum operating temperature. Many reports have demonstrated that the response of sensing materials is greatly affected by the operating temperature. Changes in operating temperature alter the kinetics of oxygen adsorption and the reaction of gases adsorbed on the sensor surface, resulting in changes of material resistance[29]. The
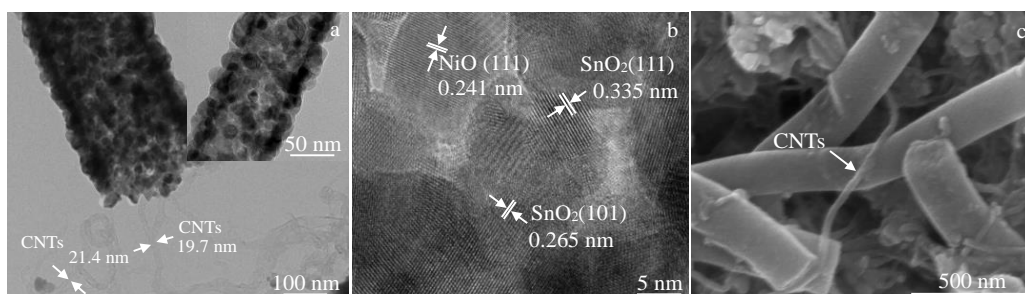

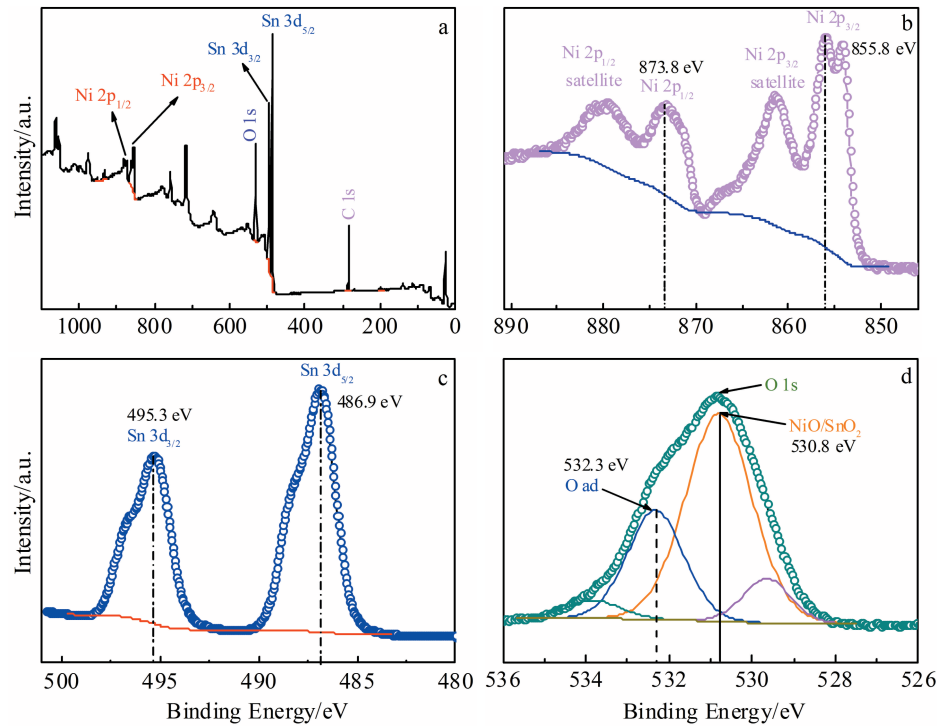Fig.5　TEM（a）and SEM（c）images of CNTs/NiO/SnO$_2$ composite fibers；HRTEM image of lattice fringes（b）

Fig.6　Survey spectra（a），Ni 2p（b），Sn 3d（c），and O 1s（d）spectra of CNTs/NiO/SnO$_2$ nanofibers
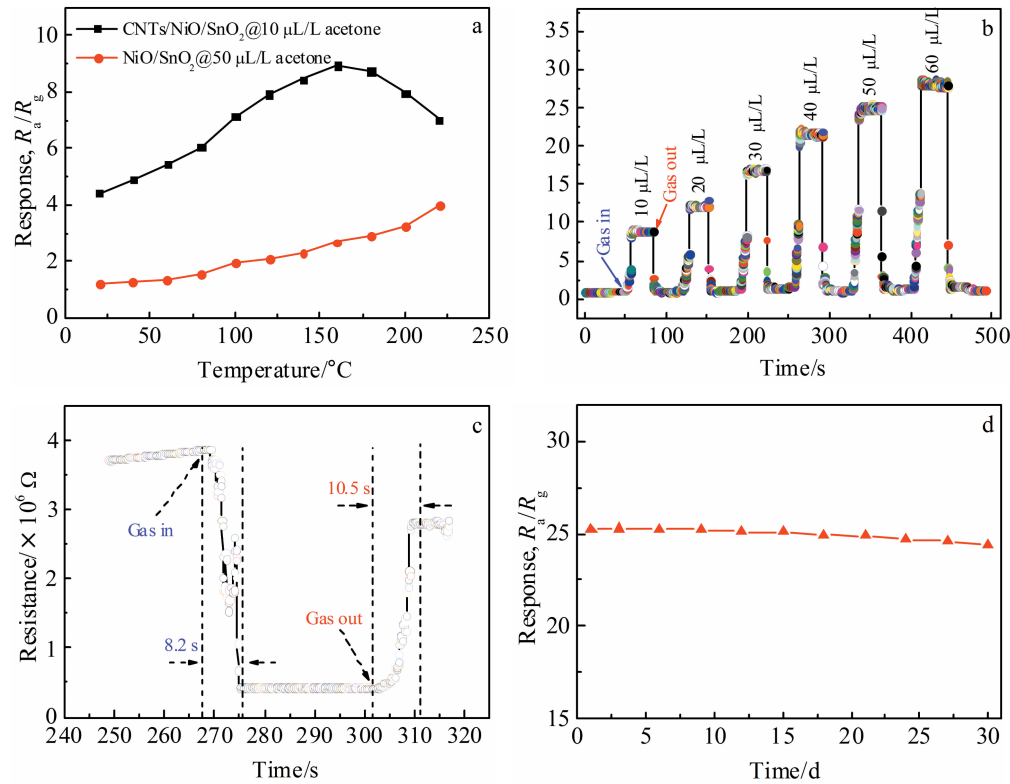

Fig.7　Response of CNTs/NiO/SnO$_2$ and NiO/SnO$_2$ sensors to acetone（a）；response-recovery behavior for the sensors at 160 °C to different con-centrations of acetone（b）；resistance change of the sensors at 160 °C under 50 μL/L acetone（c）；stability of the sensors to 50 μL/L ace-tone at 160 °C（d）

working temperature is lower than 160 °C, and the response increases as temperature increases. When it is higher than 160 °C, the response decreases with the increase of temperature, because the amount of gas adsorbed on the surface of the material decreases with the working temperature, while as the temperature arises, the desorption process becomes dominant, resulting in a decrease in response. At the temperature of 160 °C, desorption rate of the gas is equal to adsorption rate, resulting in the highest response of the sensors [30]. In addition, compared with the sensor made of NiO/SnO₂ composite material, the sensor made of NiO/SnO₂ composite material is more sensitive. Fig.7b shows the transient response of sensors based on CNTs/NiO/SnO₂ composite to different concentrations of acetone (10, 20, 30, 40, 50, 60 μL/L) at optimal operating temperature. The response value increases with the increase of acetone concentration, and the maximum response to 50 μL/L acetone reaches 25.25. To reveal the time dependence of the response, Fig.7c shows the change in resistance of the sensor to 50 μL/L acetone at the optimum operating temperature. The resistance decreases after sensors contact acetone gas, and when air flows into the test room, the resistance recovers to steady-state in the air environment, and the response/recovery time of the composite material to 50 μL/L acetone was re-

stored. The response and recovery time are 8.2 and 10.5 s, respectively. The recovery time is longer than the response time, probably due to the difficulty of the product gas (CO_2) being desorbed[30]. To further study the performance stability of the sensors, a 30 d long-term stability test was performed. As shown in Fig.7d, the sensors have good stability against acetone. Compared with the relevant research progress, as shown in Table 1, the CNTs decorated NiO/SnO₂ nanofiber material reduces the optimal working temperature, resulting in a lower energy consumption of the gas detection process, and also improves the response sensitivity. It is confirmed to be a promising sensitive material for the efficient and selective detection of volatile acetone gases.

2.3 Sensing mechanisms

The experimental results show that the sensing performance of NiO/SnO₂ decorated by CNTs to acetone is greatly improved. As shown in Fig.4a, compared with the traditional solid nanofibers, the hollow porous nanofibers prepared by electrospinning have larger specific surface area, which will be beneficial to adsorption and diffusion of gas molecules. In addition, the formation of a nano-heterojunction at the interface between the two oxides contributes to enhanced gas sensing[36]. It is known that SnO₂ mainly exhibits n-type conductivi-

Table 1   Comparison of gas-sensing properties of sensors based on various sensing materials toward acetone

Sensor materials	Concentration/μL·L⁻¹	Temperature/°C	Response，R_a/R_g	Ref.
Hollow NiO-SnO₂	50	280	4.2	[31]
Porous NiO/SnO₂ microsphere	100	240	10.1	[26]
Branched SnO₂/ZnO	100	275	9.5	[32]
Porous Co₃O₄ MR	50	200	195	[33]
NiFe₂O₄ microspheres	100	250	27.4	[15]
Pd Au/SnO₂ 3D nanosheets	2	250	6.5	[34]
ZIF-90 based QCM	20		12	[35]
CNTs/NiO/SnO₂	50	160	25.25	This work

ty by electrons, and NiO exhibits p-type conductivity through holes. As shown in Fig.8, electrons in SnO₂ and holes in NiO diffuse in opposite directions due to the carrier concentration gradient. Then, the internal electric field is formed at the NiO/SnO₂ interface, and the carrier diffusion is finally balanced[37]. When the composite is exposed to air at a high temperature, oxygen molecules in the air can be absorbed on the surface of the material and the chemically adsorbed oxygen species (O^{2-}, O^- or O^{2-}) are formed according to Eq.(1~4)[23]. The composite reacts with the exposure to acetone, according to Eq.(5) and Eq.(6).

$$O_2(gas) \leftrightarrow O_2(adsorbed) \qquad (1)$$
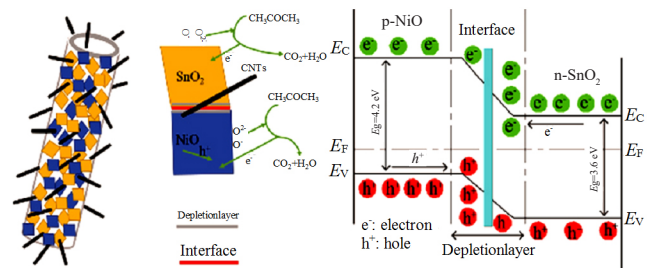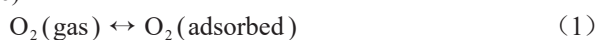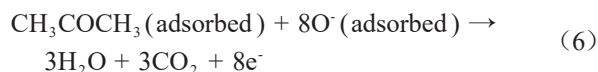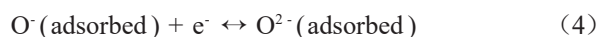

Fig.8   Response mechanism of the CNTs/NiO/SnO₂ gas sensor

$$O_2(\text{adsorbed}) + e^- \leftrightarrow O_2^-(\text{adsorbed}) \quad\quad (2)$$

$$O_2^-(\text{adsorbed}) + e^- \leftrightarrow 2O^-(\text{adsorbed}) \quad\quad (3)$$

$$O^-(\text{adsorbed}) + e^- \leftrightarrow O^{2-}(\text{adsorbed}) \quad\quad (4)$$

$$CH_3COCH_3(\text{gas}) \rightarrow CH_3COCH_3(\text{adsorbed}) \quad\quad (5)$$

$$CH_3COCH_3(\text{adsorbed}) + 8O^-(\text{adsorbed}) \rightarrow \atop 3H_2O + 3CO_2 + 8e^- \quad\quad (6)$$
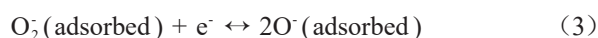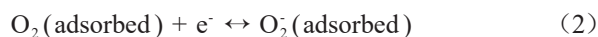
3 Conclusions

1) NiO/SnO_2 nanomaterials with hollow porous structure can be successfully prepared by electrospinning, and acidified functionalized CNTs were decorated to obtain CNTs/NiO/SnO_2 composite sensor.

2) The prepared CNTs/NiO/SnO_2 can be used as the sensing material for detecting acetone. At the optimum operating temperature of 160 °C, the sensors show high response to acetone and fast response/recovery rate. The response to 50 μL/L acetone reaches 25.25, and its response and recovery time are 8.2 and 10.5 s, respectively. At the same time, the material also has good stability.

3) The excellent sensing properties of CNTs/NiO/SnO_2 can be attributed to the introduction of nanochannels into the CNTs, the hollow porous structure of the material and the nanoheterojunction formed between NiO/SnO_2.

References

1   Xiao J K, Song C W, Dong W *et al. Rare Metal Materials and Engineering*[J], 2017, 46(5): 1241

2   Shi G L, He Y G, Luo Q W *et al. Sensors and Actuators B: Chemical*[J], 2018, 257: 451

3   Weng Y Y, Deng D Y, Zhang L C *et al. Analytical Methods*[J], 2016, 43(8): 7816

4   Wang J X, Yang J, Han N *et al. Rare Metal Materials and Engineering*[J], 2018, 47(6): 1682

5   Terra I A A, Sanfelice R C, Valente G T. *Journal of Applied Polymer Science*[J], 2018, 135(14): 46 128

6   Bagchi S, Achla R, Mondal S K. *Sensors and Actuators B: Chemical*[J], 2017, 250: 52

7   Kong J, Franklin N R, Zhou C W *et al. Science*[J], 2000, 5453(287): 622

8   Righettoni M, Amann A, Pratsinis S E *et al. Materials Today*[J], 2015, 18(3): 163

9   Hahn Y B, Ahmadw R, NTripathy *et al. Chemical Communications*[J], 2012, 84(48): 10 369

10 Righettoni M, Tricoli A, Pratsinis S. *Analytical Chemistry*[J], 2010, 82(9): 3581

11 Zhou X, Wang B Q, Sun H B *et al. Nanoscale*[J], 2016, 10(8): 5446

12 Shin J, Choi S J, Lee I *et al. Advanced Functional Materials*[J], 2013, 23(19): 2357

13 Lee J H. *Sensors and Actuators B: Chemical*[J], 2009, 140: 319

14 Sun P, Wang C, Zhou X *et al. Sensors and Actuators B: Chemical*[J], 2014, 193: 616

15 Mishra R K, Kushwaha A, Sahay P P. *RSC Adv*[J], 2014, 8(4): 3904

16 Zhang S F, Jiang W H, Li Y W *et al. Sensors and Actuators B: Chemical*[J], 2019, 291: 266

17 Liu X J, Zhao K R, Sun X L *et al. Sensors and Actuators B: Chemical*[J], 2019, 290: 217

18 Wen A, Yang C Y. *Applied Mechanics and Materials*[J], 2011, (143-144): 562

19 Kemmler J A, Pokhre S l, Maedler L *et al. Nanotechnology*[J], 2011, 44(24): 442 001

20 Huang J, Wan Q. *Sensors*[J], 2011, 12(9): 9903

21 Patil G E, Kajale D D, Gaikwad V B *et al. Journal of Nanoscience and Nanotechnology*[J], 2012, 8(12): 6192

22 Fan J, Liu P, Chen X H *et al. Nanotechnology*[J], 2019, 30: 475 501

23 Zhang W S, Fan Y, Yuan T W *et al. ACS Applied Materials & Interfaces*[J], 2020, 12(3): 3755

24 Choi S, Park J Y, Kim S S. *Chemical Engineering Journal*[J], 2011, 172(1): 550

25 Zhang Z Y, Wen Z, Ye Z Z *et al. RSC Advances*[J], 2015, 74(5): 59 976

26 Gu C P, Cui Y W, Wang L Y *et al. Sensors and Actuators B: Chemical*[J], 2017, 241: 298

27 Zhang S S, Li Y W, Sun G *et al. Sensors and Actuators B: Chemical*[J], 2019, 288: 373

28 Zhao B, Ke X K, Bao J H *et al. The Journal of Physical Chemistry C*[J], 2009, 113(32): 14 440

29 Zhu L Y, Yuan K, Yang J G *et al. Sensors and Actuators B: Chemical*[J], 2019, 290: 233

30 Bai S, Guo W, Sun J *et al. Sensors and Actuators B: Chemical*[J], 2016, 226: 96

31 Wang L L, Deng J N, Fei T *et al. Sensors and Actuators B: Chemical*[J], 2012, 164(1): 90

32 Yang X, Zhang S, Yu Q *et al. Sensors and Actuators B: Chemical*[J], 2019, 281: 415

33 Wang S M, Cao J, Cui W *et al. Sensors and Actuators B: Chemical*[J], 2019, 297: 126 746

34 Li G J, Cheng Z X, Xiao Q *et al. Sensors and Actuators B: Chemical*[J], 2019, 283: 590

35 Zhang D, Fan Y, Li G J *et al. Sensors and Actuators B: Chemical*[J], 2020, 302: 127 187

36 Ju D X, Xu H Y, Qiu Z W *et al. Sensors and Actuators B: Chemical*[J], 2014, 200: 288

37 Chen Y, Yu L, Feng D *et al. Sensors and Actuators B: Chemical*[J], 2012, (166-167): 61

碳纳米管修饰的空心多孔 NiO/SnO₂ 纳米复合材料对丙酮传感性能的优化

周洪雷，陈小红，范　军，刘　平

(上海理工大学 材料科学与工程学院，上海 200093)

摘　要：通过静电纺丝法制备中空多孔的 NiO/SnO₂ 复合纳米纤维，在复合纤维表面装饰碳纳米管，在此基础上制备气敏传感器器件。利用 TGA 确定了复合材料热分解温度和热处理工艺；利用 SEM、XRD、TEM、XPS 分别对复合材料的形貌、结构、尺寸、表面成分进行了表征。使用 WS-30A 气敏元件测试仪对气敏元件响应进行了测试。结果表明，CNTs 修饰的 NiO/SnO₂ 复合纳米材料制备的气敏传感器降低了丙酮检测的最佳工作温度为 160 ℃，提高了检测灵敏度，对 50 μL/L 丙酮的响应达到 25.25，对检测丙酮有快速的响应（~8.2 s）以及恢复性能（~10.5 s），同时在 30 d 的长期稳定性测试中也体现了良好的稳定性。证明了装饰 CNTs 的 NiO/SnO₂ 复合材料在检测丙酮方面的潜在价值，同时也进一步讨论了 CNTs，中空多孔结构的 NiO/SnO₂ 提高检测性能的作用机理。

关键词：NiO/SnO₂；半导体；碳纳米管；气体传感器

作者简介：周洪雷，男，1981 年生，博士，上海理工大学材料科学与工程学院，上海 200093，E-mail: zhouyutian007@163.com